Applied Physics A (2020) 126:395
https://doi.org/10.1007/s00339-020-03558-7

Applied Physics A
Materials Science & Processing

S.I. : CURRENT STATE-OF-THE-ART IN LASER ABLATION

Effect of ambiance on the coal characterization using laser-induced breakdown spectroscopy (LIBS)

Hemalaxmi Rajavelu[1] · Nilesh J. Vasa[1] · Satyanarayanan Seshadri[2]

Received: 15 October 2019 / Accepted: 16 April 2020 / Published online: 7 May 2020

Abstract

The influence of surrounding gases, such as He, N_2, atmospheric air, and Ar, and gas flow rate on the laser-induced breakdown spectroscopy (LIBS) characterization of coals in free space is studied. The atomic and molecular carbon (C_2 and CN) emission intensities are observed to be higher in Ar and N_2 ambiance. Quantitative analysis of carbon and ash content in different coal samples is carried out using the carbon bound atomic and molecular emission signals and the ash forming elements (Si, Fe, Mg, Al, Ca, Na, and K) signals. The sum of the LIBS emission of the all and major ash forming elements increased linearly with an increase in the ash content. Similarly, the ratio between the carbon signals (C I, CN, and C_2) and the sum of major ash forming elements (Si, Al, Fe, and Ca) also showed a linear increase with the increase in carbon content in coal samples. The linear coefficient of regression, R^2, was estimated to be 0.67, 0.58, and 0.85, and the root mean square of calibration samples was estimated to be 5.71, 5.82, and 5.57 wt% using the partial least square regression (PLSR) method for air (no flow), N_2, and Ar atmosphere, respectively. The precision and accuracy of the carbon measurement in coal samples by the LIBS technique using the PLSR method were higher in the presence of Ar than air or N_2 atmosphere due to the plasma shielding effect.

Keywords LIBS · Coal · Coal ash · Elemental analysis · Gas flow

1 Introduction

The chemical composition of coal has a significant impact on coal-fired thermal power plants and boiler performance, where the physical and chemical behavior of coal can influence the combustion process [1]. Ultimate and proximate analyses are the current state of the art for analyzing the composition, which is an off-line and time-consuming process (often, the analysis can take up to 8 h) [2]. Other techniques like X-ray fluorescence spectroscopy (XRF) and prompt gamma neutron activation analysis (PGNAA) can provide fast online analysis [3, 4]. However, XRF cannot detect light elements, and PGNAA requires strict safety regulations because of the radioactive neutron source. Alternatively, laser-induced breakdown spectroscopy (LIBS), which uses pulsed laser ablation to form plasma over the target surface and involves optical emission-based measurements, can also be considered for the elemental analysis. LIBS technique is the better choice for online coal monitoring as it offers fast real-time measurement and requires minimal sample preparation [5].

LIBS technique captures the plasma emission from the target, which is majorly formed due to atomic emissions from the target. Various research groups have attempted the LIBS technique for coal analysis [6–9]. LIBS has also been used for fly ash analysis and screening of additives to mitigate fouling deposits in coal-based power plants [10]. Most of the studies on coal analysis involve atomic emissions of various elements in coal samples, such as C, Si, Mg, Al, Fe, Ca, Ti, Na, H, K, O, and N. During LIBS, molecular emissions like CN and C_2 are also observed. The reasons for molecular signals are direct fragmentation, the reaction of the excited species in the plasma, and the reaction between the excited species with the surrounding gas atmosphere [11, 12]. LIBS technique involves calibration of the elements for

✉ Nilesh J. Vasa
njvasa@iitm.ac.in

Hemalaxmi Rajavelu
hemarajavel20@gmail.com

[1] Department of Engineering Design, Indian Institute of Technology Madras, Chennai 600036, India

[2] Department of Applied Mechanics, Indian Institute of Technology Madras, Chennai 600036, India

the quantitative analysis to improve the precision of measurement [13, 14]. In LIBS, measurement accuracy also depends on the physical and chemical structure of the target, gas environment. LIBS analysis and elemental estimation in the air environment are also expected to be influenced by the oxidation of species of interest during the LIBS. In the case of LIBS-based coal analysis, the surrounding gas environment significantly affects the optical emission and plasma properties (plasma temperature and electron density) [15–17]. Few studies reported the effect of the surrounding gas, such as Ar, He, and air atmospheres on the LIBS signal of coal by keeping the coal pellets inside a vacuum chamber [12, 18]. However, the approach may have limitations concerning an online coal monitoring system.

Alternatively, an appropriate gas may be fed over the target to surround the ablation region. This approach can protect the ablation region by preventing exposure to the uncontrolled ambiance and the influence of atmospheric contaminants. Also, it can remove the coal particles, which may disintegrate from the sample during the laser ablation and interfere with both the incoming laser pulses and plasma emission. The surrounding flow gas is also expected to interact with plasma generated during the laser ablation and influence the atomic emission and molecular emission spectra. As a result, all atomic and molecular emission lines concerning carbon elements can also be considered with emission lines of other major ash forming elements to improve the measurement accuracy in the quantitative analysis. Hence, in the present study, the LIBS technique with flow gases in free space is proposed and demonstrated for a possible online coal analysis application. No such studies have been conducted in free space to understand the influence of the surrounding gas and its flow near the atmospheric pressure on LIBS intensity, characterization, and quantitative analysis of coal. In this work, the characteristics of carbon bound atomic and molecular emissions (C I, CN, and C_2) and ash elements during the LIBS analysis of coal samples under He, N_2, Air, and Ar flow conditions are studied spectrally in free space. Quantitative analysis of carbon content in different coal samples is also carried out by using the carbon bound atomic and molecular signals and the ash forming element signals.

In Sect. 2, the LIBS experimental setup for the coal characterization in a controlled gas flow environment is described. Section 3 explains the effect of gas flow on LIBS spectra and the characteristic emissions. Based on the LIBS spectra of 19 coal samples, quantitative analyses concerning carbon content are performed and validated in normal ambiance (atmospheric air), nitrogen, and argon gas flow conditions. The performance of the methods adopted for the C measurement was evaluated by the following parameters: R^2 of the linear fit line w.r.t the reference C value, root mean square error of calibration (RMSEC), root mean square error of validation (RMSEV), and relative standard deviation (RSD). Finally, conclusions are described in Sect. 4.

2 Experimental setup

Figure 1 shows the schematic diagram of the LIBS experimental setup. A Q-switch Nd^{+3}: YAG laser with 10 ns pulse width, 10 Hz repetition rate, and 30 mJ pulse energy at 1064 nm wavelength was focused on the coal samples using a plano-convex lens with a focal length of 150 mm. The coal samples were placed on a stage mounted on a rotary stepper motor. The optical emission from the plasma was coupled to a low-OH optical fiber (core diameter: 500 µm, numerical aperture: 0.22) by a plano-convex lens with a focal length of 100 mm. The optical emission was fed to the spectrometer by the optical fiber. The complex chemical composition of coal shows emission from 190 to 800 nm comprising all the neutral atomic emissions of various elements present in it.

When UV–Vis–NIR spectrometer (180–850 nm, ≈1–2 nm resolution) (USB2000+, Ocean Optics) was employed for the LIBS study, it was possible to observe emissions across the whole range. However, since the resolution was compromised, it was difficult to resolve C and Si emission lines near 247 nm. Further, the spectral sensitivity of the spectrometer was lower in the UV region. Hence, a spectrometer (173–430 nm, 0.3 nm resolution) (FREEDOM HR-DUV, Ibsen Photonics) was used to improve the resolution and sensitivity in measurements in the UV range. Both the laser and the spectrometers were kept synchronized by the delay generator to ensure the minimum coupling of an initial continuum light from the plasma. Approximately, 2-µs delay was maintained by using the Q-switched triggering signal from the laser source. The gate delay of 2 µs was selected based on the signal-to-background ratio (S/B) and signal-to-noise ratio (SNR) of time-resolved LIBS analysis

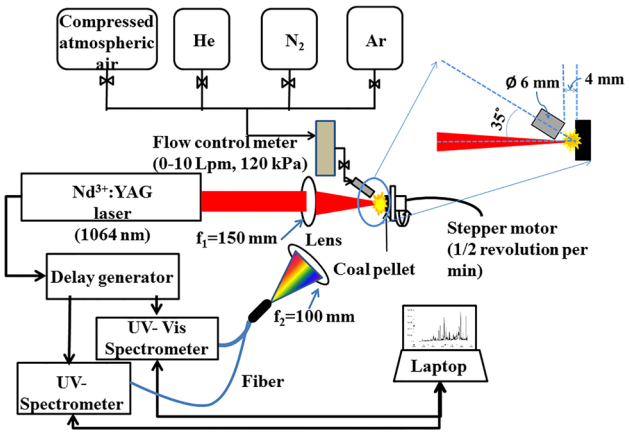

Fig. 1 Schematic diagram of the LIBS experimental setup

of a coal sample done in the air. LIBS measurements were performed in the different ambiances by supplying a gas (He, N_2, Air, or Ar) through a polyurethane (PU) tube (6 mm diameter) held at 4 mm above the surface of the target. The PU tube was held at an angle of 35 ° from the laser beam, as shown in Fig. 1, so that the expanding gas at the outlet reaches the ablation spot. The gas flow was controlled using a rotameter from 0 to 10 Lpm (liter per minute) at the supply pressure of ≈120 kPa.

Nineteen numbers of coal samples were used for the analysis, out of which 15 samples were used for calibration, and four (randomly selected) samples were used for validation. 13 samples were raw coal of different shapes, and six samples were compacted coal pellets (pulverized coal samples made into solid targets). The six powder samples were compacted into pellets of 40 mm diameter and 7 mm thick in a hydraulic press by applying a pressure of 200 MPa pressure. The target was rotated with the help of a stepper motor stage to capture the LIBS spectrum from different regions on the target. The rotating speed of approximately ½ revolution per minute provided a fresh location on a sample for each laser pulse. Each measurement was performed 50 times to reduce the influence of temporal fluctuations due to the small variation in the laser energy, the surface variation of samples, and the corresponding plasma emissions.

The 19 coal samples were also characterized using C–H–N–S analysis (LECO, Truspec Micro Analyzer) to determine elemental C, H, N, and S content. The elemental content of each coal sample was also measured thrice using C–H–N–S analysis. Each sample was made into powder and sieved to 150 µm sized for the analysis. Ash concentration (wt.%) was obtained based on the proximate analysis results. The elemental carbon content and the ash content of the 19 coal samples are listed in Table 1. C–H–N–S measurements were performed three times, and the average concentration (wt%) and error in measurements in terms of standard deviation (wt%) were estimated and are included in Table 1. In some samples, this variation was ≈10 wt% and the average standard deviation of error was estimated to be around 4 wt%. The large error in the measured carbon concentration was attributed to the spatial variation in the carbon concentration of a coal sample.

3 Results and discussion

3.1 LIBS spectra

Figure 2a and b shows the LIBS spectra of a coal sample in the 173–430 nm and 180–850 nm ranges under different ambiance gases (He, N_2, Air and Ar) at 1 Lpm (liter per minute) flow rate. The LIBS spectrum was matched with the NIST LIBS database for the elemental identification, and the molecular signals were confirmed from reference [11, 12, 19]. Figure 2 shows the presence of atoms, namely C, Si, Mg, Al, Fe, Ca, Na, O, H, and K, molecular signatures of CN, and C_2. These measurements are shown without incorporating spectral sensitivity of the measurement system including optical coupling and spectrometers. The spectral characteristics were different under various ambiances due to the physical and chemical behavior of the plasma changes for different gas species. From Fig. 2, the LIBS spectral intensity was the highest in the Ar environment and the lowest in the He environment. The LIBS spectra in the case of no flow (atmospheric condition), compressed air flow and N_2 flow conditions were similar, which can be attributed to the influence of the density and the atomic mass of the surrounding gas on the material ablation and plasma confinement.

The influences of the surrounding gas result in the cascade-like growth of the number density of the emitting

Table 1 Elemental carbon and ash content of coal samples

Sample name	Elemental carbon (wt%), error (± wt.%)	Ash (wt%)	Sample name	Elemental carbon (wt%), error (± wt.%)	Ash (wt%)
Calibration set			K	56.4, 0.4	16.2
A	32.6, 1.9	41.4	L	62.7, 0.9	3.3
B	52.8, 0.2	33.7	M	40.6, 2.2	38.4
C	56.9, 0.3	22.5	N	54.7, 1.0	26.5
D	49.6, 4.1	36.8	O	48.6, 1.4	33.1
E	38.2, 4.6	20.8	Validation set		
F	44.0, 1.7	40.6	P	53.1, 4.9	40.9
G	53.7, 0.9	10.7	Q	48.1, 2.8	31.7
H	53.4, 9.0	20.1	R	52.4, 0.6	43.4
I	54.3, 1.1	23.2	S	43.1, 1.1	40.3
J	66.3, 3.2	2.5			

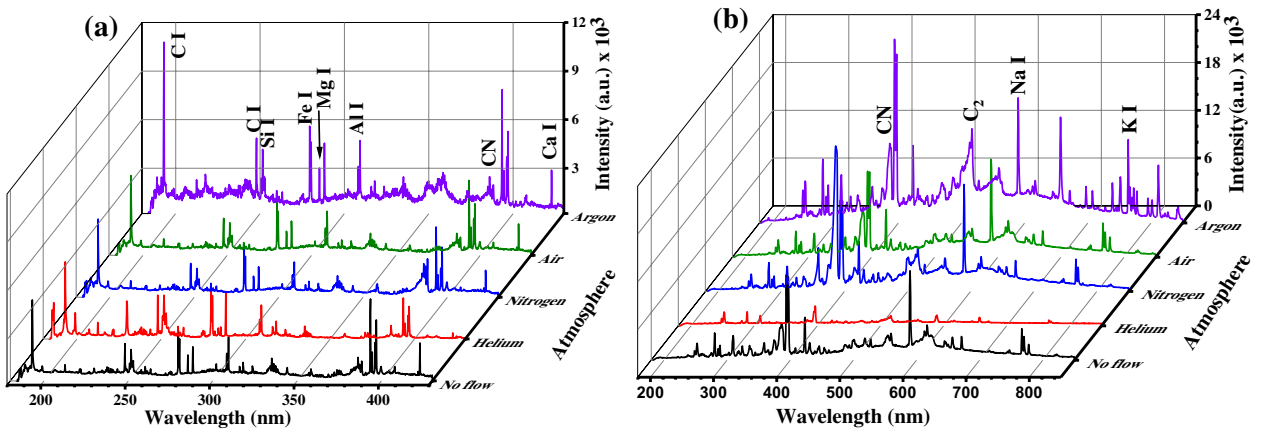

Fig. 2 Emission spectra of coal observed during laser ablation at the absence of gas flow and He, N_2, Air, and Ar gas flow conditions in the wavelength range of **a** 173–430 nm and **b** 180–850 nm

Table 2 Physical parameters of different atmospheric gases

Parameters	Ar	Air	N_2	He
Density (g/L)	1.78	1.28	1.25	0.18
Thermal conductivity (W/cm. K) $x\ 10^4$	1.77	2.62	2.60	15.67
Ionization potential (eV)	15.75	N_2: 14.53 O_2: 13.62	14.53	24.58
Atomic weight (g/mol)	39.95	N_2: 28.01 O_2: 32.00	28.01	4.00
E/M	0.39	0.49	0.52	6.14

species in the plasma, and the necessary condition for the cascade-like plasma growth is given by Eq. 1 [20]:

$$\frac{d\varepsilon}{dt} = \frac{4\pi^2 e^2 I \upsilon_{eff}}{m_e c \omega^2} - \frac{2 m_e \upsilon_{eff} E}{M} \quad (1)$$

where ε is the energy of free electrons, m_e and e are the mass and charge of the electron, M is the mass of the neutral gas particle, E is the ionization potential of the first ionization stage of the gas, I and ω are the intensity and cyclic frequency of the source and υ_{eff} is the effective frequency of electron-neutral collisions. The first term on the right side in Eq. 1 represents the interaction of laser energy to the target, which remains the same for all the gases. The second term explains the rate of energy loss in the plasma due to the elastic and inelastic collisions of plasma with the neutral gas particles. The *E/M* ratio of the surrounding gas influences the cascade-like plasma growth, which is described in Table 2. Table 2 lists the density, thermal conductivity, ionization potential, atomic weight, and E/M ratio of the different surrounding gas species [18]. Based on Table 2, the *E/M* ratio is very close in the case of air and N_2, and hence, the characteristics of the plasma growth are expected to be approximately the same. The *E/M* ratio was estimated to be the lower in Ar and higher in He. In the experimental study, the optical emission intensity in He environment was reduced. He gas has a higher ionization potential (24.59 eV), which would also permit improved energy absorption by the material via inverse bremsstrahlung, and the optical emission intensity was expected to increase to a certain extent. However, rapid plasma expansion due to the lower density and mass of He (high *E/M* ratio) might have contributed to a signal with a large amplitude but a shorter duration. As a result, a reduction in the emission intensity was observed. In the case of Ar ambiance, both the emission intensity and the continuum intensity were increased. The reduced *E/M* ratio was expected to increase the cascade-like plasma growth and hence the energy transfer via inelastic collisions resulting in a prolonged emission. Hence, near the atmospheric pressure, emission intensity in Ar was higher than Air, N_2, and He. However, background continuum emission intensity was also increased as shown in Fig. 2a and b.

3.2 Effect of gas flow rate

To understand the effect of gas flow rate on the LIBS emission of coal, the intensities of atomic (C I—193.03 nm, and 247.8 nm) and molecular (CN—388.34 nm and C_2—516.32 nm) carbon emissions were studied. The intensities were corrected with the spectral sensitivity of both spectrometers. Figure 3a, b, c, and d shows the behavior of the atomic C I emission at 193.03 nm and 247.8 nm and molecular CN emission at 388.34 nm and C_2 emission at 516.32 nm, respectively, in He, N_2, air, and Ar environment with a gas flow rate from 0 to 10 Lpm. In the case of compressed air flow, atomic C I and molecular C_2 emission intensities as shown in Fig. 3a, b, and d remained almost the

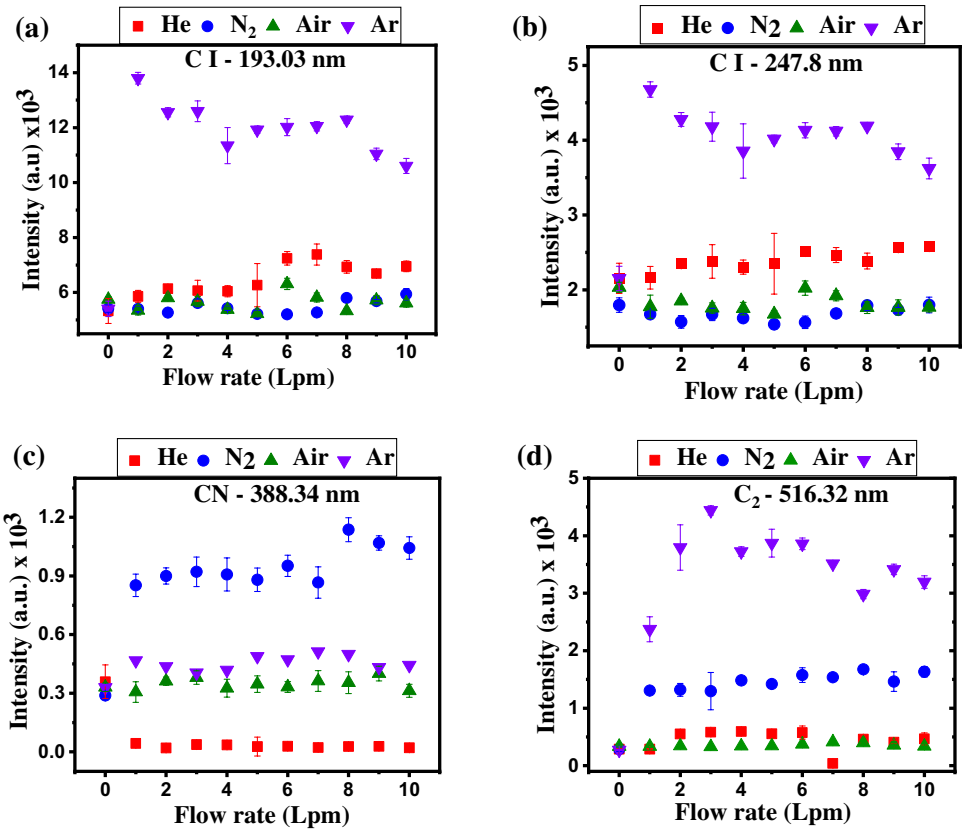

Fig. 3 Emission characteristics of **a** atomic carbon C I—193.03 nm, **b** C I—247.8 nm, **c** molecular CN, and **d** C_2 w.r.t flow rate under various gas flow

same with different flow rates. Nevertheless, the molecular CN signal was slightly improved, as shown in Fig. 3c. In the case of N_2 gas flow, almost similar trends were seen for atomic C I and molecular C_2 emission intensity, as shown in Fig. 3a, b, and d, respectively. Nevertheless, as shown in Fig. 3c, in N_2 environment, the molecular CN signal was higher compared to the other gas environments. This may be due to the surplus supply of nitrogen to the ablation region, enhancing the reaction between the excited carbon in the plasma and the surrounding N_2 gas molecules by the reaction $C + N_2 \leftrightarrow CN + N$ at the periphery of the plasma. Also, as shown in Fig. 3(d), the formation of C_2 species by the reaction of $C + CN \leftrightarrow C_2 + N$ improved the signal strength in the case of N_2 than air [12]. Further, the use.

of gas flow at lower flow rates around 1–2 Lpm was suitable for allowing settling of coal dust particles without much interference with the subsequent laser ablation pulses.

As shown in Fig. 3, the Ar environment resulted in higher emission intensities than the air, N_2, and He environment except for the case of CN emission intensity. In the Ar environment, the interaction of atmospheric N_2 with the plasma was avoided and the increased ablation rate of bound CN radicals from the target resulted in a slightly higher CN intensity than in air. Also, with the increase in the Ar flow rate of more than 1 Lpm, a drop in the emission intensities was observed. This can be attributed to the plasma shielding effect at higher flow rates. As shown in Fig. 3, He environment resulted in a lower emission intensity compared to the other environments. However, the atomic C I emission intensity was higher than that in the air and N_2 environment, as the atomic carbon was not involved in the formation of CN and C_2 radicals.

3.3 Plasma temperature and electron density

The plasma temperature and electron density were calculated by considering the plasma is in the local thermodynamic equilibrium (LTE) state. In this study, the plasma temperature T_e was evaluated using the spectral intensities of typical neutral atomic emission lines of Si at 212.4 nm and 251.6 nm using the line pair method as given in Eq. 2 [21, 22]:

$$T_e = 1.44 \frac{E_2 - E_1}{\ln\left[\frac{I_1 \lambda_1 A_2 g_2}{I_2 \lambda_2 A_1 g_1}\right]} \quad (2)$$

where, E_1, A_1, g_1, and I_1 are the upper energy level, transition probability, statistical weight of the upper state, and the spectral intensity at λ_1, respectively. E_2, A_2, g_2, and I_2 are the similar parameters at λ_2. The modified Saha equation (Eq. 3) was used to determine the electron density, which involves

the ion–atom intensity ratio [23]. The neutral atomic line at 251.43 nm (Si I) and the first ionized emission line at 207.2 nm (Si II) were substituted in Eq. 3 to find the electron density n_e:

$$n_e = \frac{I_a}{I_i} \times 6.6 \times 10^{21} \frac{A_i g_i}{A_a g_a} \exp\left(-\frac{E^{ion} + E_i - E_a}{T_e}\right) \quad (3)$$

where E^{ion} is the first ionization potential of Si ($E^{ion} = 8.1517eV$). E_i and E_a are the energies of the upper states corresponding to Si II and Si I, respectively. The spectroscopic properties of Si lines used in the measurement are listed in Table 3. The calculated plasma temperature and electron density with different gas flow conditions (He, N_2, air, and Ar) are shown in Fig. 4a and b, respectively.

From Fig. 4a and b, both T_e and n_e values are higher in the presence of Ar, N_2, air, and He. The above results explain that the plasma temperature and electron density play a significant role in the plasma emission characteristics in different gas atmospheres, mainly with Ar and He. The expansion rate of the plasma can vary for different gases because of its gas density and atomic number as mentioned in Table 2. Since the density and atomic weight of Ar gas are the highest, the plasma is confined, which leads to the higher T_e and n_e. The higher electron density in a plasma plume will absorb a significant portion of the incoming laser energy which results in an increased rate of electron collision and plasma temperature in the Ar atmosphere. The above process improves the atomic line strength by collisional excitation and re-excitation in the presence of Ar gas. The lower atomic weight and gas density in N_2, air, and He result in faster expansion of plasma plume because the background gas provides less momentum drag. Therefore, the plasma emission intensity, temperature, and electron density were maximum in Ar atmosphere but gradually decreased in the presence of N_2, air, and He, respectively.

Table 3 Spectral information of neutral and ionized Si states from the NIST database

Species	Wavelength λ (nm)	Upper-level energy E (eV)	Einstein Coefficient A (s^{-1}) x 10^8	Upper-state degeneracy g
Si I	212.41	6.61	2.9	7
Si I	251.43	4.95	1.68	5
Si II	207.20	12.83	1.0	8

3.4 Effect of atmosphere on the S/B ratio

A background continuum emission was also observed along with LIBS emission intensity. The continuum emission depends upon the interacting laser fluence and the surrounding atmosphere. Hence, the effect of the surrounding environment on the signal-to-background (S/B) ratio was studied. The S/B ratio is estimated using the formula $(I_s - I_b)/I_b$ [24], where I_s is the peak intensity of an element line and I_b is the intensity of the background emission. The S/B ratio was estimated for all major element emission lines in the different gas environments with a typical flow rate of 1 Lpm. Figure 5 shows the S/B ratio estimated with He, N_2, air, and Ar flow environments. The main reason for plasma continuum emission is the bremsstrahlung radiation. The strength of the bremsstrahlung emission per unit frequency, per unit time, and per unit volume at a specific frequency (υ) is given by Eq. 4 [25, 26]:

$$I_{brems}(\upsilon) = \frac{e^6 n_e}{24\pi^2 c^3 \varepsilon_0^2 m_e K_B T} \sqrt{\frac{K_B T}{m_e}} e^{-h\upsilon/K_B T} \sum_m n_m z_m^2 \quad (4)$$

where e is the charge of the electron, c is the velocity of light in vacuum, m_e is the electron mass, n_e and n_m are the electron and ion density, respectively. ε_0 is the permittivity of vacuum, z_m is the atomic number, T is the plasma temperature and h and K_B is the Plank and Boltzmann constant, respectively. From Eq. 4, the strength of bremsstrahlung radiation depends on the electron density and the plasma temperature by considering the other parameters as constant. Based on

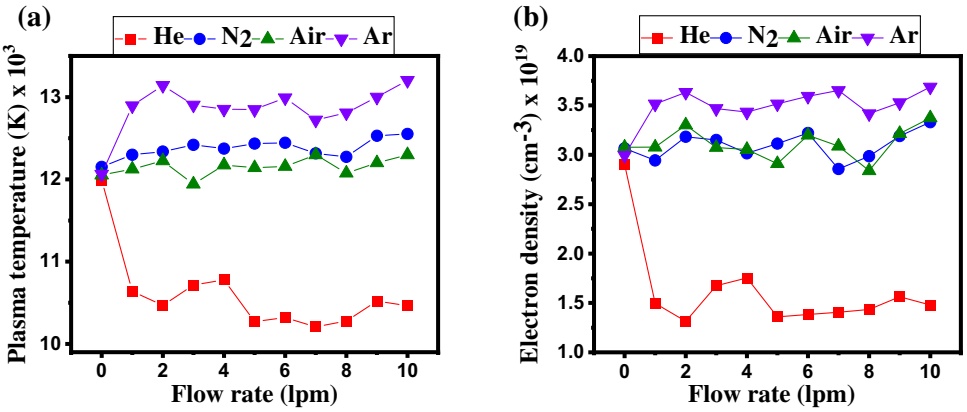

Fig. 4 **a** Plasma temperature and **b** electron density measured using atomic and ionic Si lines for different gas flow conditions (He, N_2, air, and Ar)

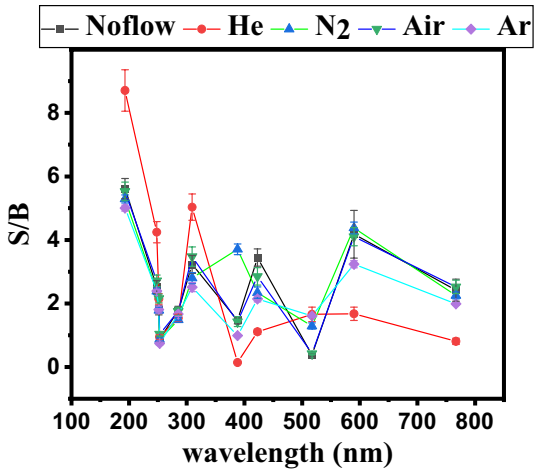

Fig. 5 Signal-to-background ratio of different emission lines used for the qualitative analysis of carbon and ash

the experimental measurements, both the plasma temperature and electron density decreased with the change in the environment in the order of Ar, N_2, air, and He, while, based on Table 2, the E/M ratio increases with the change in the environment in the order of Ar, air, N_2, and He, respectively. Hence, it can be deduced that the plasma continuum emission is highest with Ar and lowest with the He atmosphere. In the UV region, the S/B ratio was higher in He environment than that of in Ar, air, and N_2 environment as shown in Fig. 5. However, in the visible region, the S/B ratio was reduced significantly in the He environment. The reduction of signal-to-background (S/B) ratio in the visible region of the LIBS spectra for He environment was attributed to the reduced collisional ionization resulting in less background continuum radiation emission. However, in the UV region, due to the less influence of the inverse bremsstrahlung, the background radiation was expected to decrease and hence the S/B ratio for He environment in the UV region was high. On the other hand, in the case of Ar, N_2, and air environment, a very small increase in the S/B ratio in the UV region was observed; however, it was not as significant as in the case of He environment.

3.5 Quantitative analysis

To compare the influence of gas flow on the coal plasma and its characteristic emission, all the experimental parameters, namely laser energy, focusing optics, spectrometer gate delay, feed-gas flow rate, and pressure, were kept constant except the gas environment. The spectral intensity from different atomic (C I, Si I, Fe I, Al I, Ca I, Mg I, Na I, and K I) and molecular signals (CN and C_2) were measured in different ambiances, namely atmospheric air with no flow condition, N_2, and Ar environment. From the NIST LIBS database, the

Table 4 Wavelength of each element employed in the carbon measurement based on the NIST LIBS database

Element	Wavelength (nm)	Element	Wavelength (nm)
C I	193.04	Mg I	285.19
C I	247.84	Al I	309.25
CN	388.34	Ca I	422.64
C_2	516.32	Na I	589.9
Si I	251.56	K I	766.67
Fe I	252.62		

spectroscopic parameters of each elemental spectral line used in the carbon measurement are listed in Table 4. These emission intensity values were used for the quantitative analysis of different coal samples and their ash content. The LIBS emission intensities used in the analysis were background-subtracted and corrected for the spectrometer sensitivity. The partial least square regression (PLSR) method was employed for the measurement of carbon content using the various atomic and molecular signals from the LIBS spectrum of different types of coal. The analysis was performed using three cases: (i) only considering emission lines of C (atomic and molecular), (ii) emission lines of carbon, minor, and major ash elements, and (iii) emission lines of carbon and major ash elements, and results were compared.

The influence of the major and minor ash elements in the carbon measurement was studied by considering the ratio of individuals of carbon signals and the sum of major and minor ash elements. The uneven shape and size of the coal sample may introduce errors by the changes in the laser target working distance (changes in ablation fluence and collection efficiency). The normalized LIBS intensity was considered by dividing each carbon emission intensity by the sum of LIBS signals of inorganic elements to minimize the error caused by both the different sizes and the heterogeneous chemical composition of the raw coal sample used in the study. The performance was compared by estimating statistical parameters, namely R^2 of the linear fitting; root mean square error in calibration, RMSEC; root mean square error in verification, RMSEV; and relative standard deviation, RSD values for measurements in a different environment, and ash elements.

Figure 6 shows the measured C content (wt%) by the PLSR model using the atomic (C I—193.04 nm, C I—247.84 nm) and molecular carbon (CN—388.34 nm, and C_2—516.32 nm) emission in the different gas environments and the corresponding reference carbon content (wt%) of different coal samples. The performance of the measurement is compared in Table 5. The R^2 (0.01) of the calibration plot was quite poor, with no flow condition than N_2 (0.49) and Ar (0.72). Also, the RMSEC, RMSEV, and RSD of prediction were compared with no flow, N_2, and Ar environment in Table 5. The measurement technique was expected to improve by including the

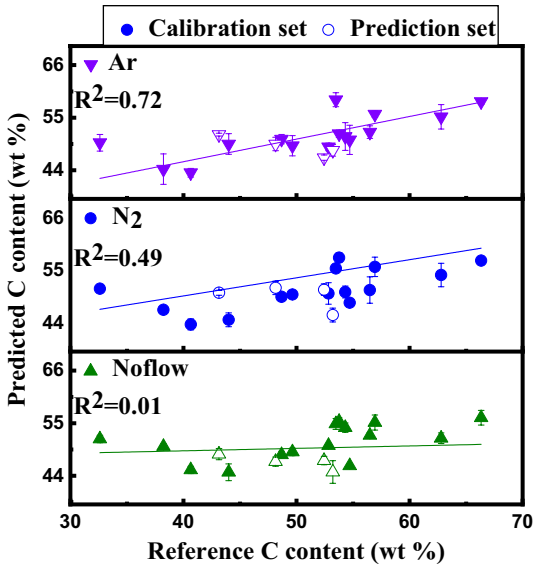

Fig. 6 Calibration plots using the individual LIBS intensities of carbon emissions (C I—193.04 nm, C I—247.84 nm, CN—388.34 nm, and C_2—516.32 nm under no flow, N_2, and Ar flow conditions) using the PLSR method

influence of the variation in percentage concentration of ash elements. The coal mainly consists of carbon and inorganic elements [consisting of major elements, such as Si; Ca; Fe; Al, and minor elements, such as Mg; Na; K (< 5% in ash)]. Therefore, for the carbon analysis, the LIBS signals of both the carbon and the inorganic elements were considered.

The coal ash is composed of various inorganic elements such as Si, Al, Fe, Ca, Mg, Na, and K. The approximate wt% of inorganic elements present in a typical coal ash which consists of Si_2O_3, Al_2O_3, Fe_2O_3, CaO, MgO, Na_2O, and K_2O is 40–70%, 10–30%, 5–20%, 5–20%, 0.5–3%, < 1%, and < 1%, respectively [27, 28]. Online ash concentration measurement considering the weighted sum of all detected inorganic elements has been reported elsewhere [29]. The elements are expected to contribute differently to the ash content and have different emission-line strengths. Similarly, in the present analysis, the sum of the emission intensity of the inorganic elements (neutral atomic emission lines) was considered for the representation of coal ash content. Based on the overall ash composition, the inorganic elements can be grouped as major (Si, Fe, Al, and Ca) and minor (Mg, Na, and K) ash forming elements. The total concentration of minor elements, such as Mg, Na, and K, was expected to be less than 5 wt%. However, due to the prominent emission lines of Mg, Na, and K, a small error or variation in the concentration (the concentration of minor elements in ash is less than 5%) was expected to result in a large difference in the LIBS spectral intensity.

Figure 7a and b shows the relation between the sum of the elemental emission intensity values of ash forming elements of coal samples and their corresponding ash content (weight percentage, wt%) estimated using the proximate analysis in different samples gas environment, namely atmospheric air (no flow), N_2, and Ar environment. By comparing Fig. 7a and b, it was observed that the measurement correlation with the actual ash content was improved by considering emission intensities of both major and minor elements. Based on Fig. 7a, a better correlation between the actual ash concentration and the sum of emission-line intensities was obtained in no flow (air atmosphere) and the Ar environment as compared to that of the N_2 environment.

Figure 8 shows the calibration plots for the carbon measurement by the PLSR model using the ratio between the individual LIBS intensity of atomic and molecular C emissions (C I, CN, and C2) and sum intensity of (a) the major and minor and (b) only the major ash elements in different gas environments. The raw coal consists of fixed carbon, volatile organic matter, moisture, and ash, and their typical wt% is 20–50%, 20–50%, 10%, and 5–50%, respectively [27]. Hence, the major components of coal samples were carbon and ash. Therefore, the ratio of LIBS signals of C and the sum of major ash elements shows a better linear relationship between the LIBS signal and the reference carbon content. Comparing the results (Fig. 8a and b), the second method considering only the major ash content shows better linearity between the measured C value and the reference C value of various coal samples in the air (no flow), N_2, and Ar environment. As observed from Table 5, the R^2, RMSEC, RMSEV, and

Table 5 Comparison of the LIBS techniques combined with PLSR for the C measurement

	No flow			N_2			Ar		
Method adopted →	*C* only	*C*, major, minor elements	*C*, major elements	*C* only	*C*, major, minor elements	*C*, major elements	*C* only	*C*, major, minor elements	*C*, major elements
R^2	0.01	0.57	0.67	0.49	0.59	0.58	0.72	0.57	0.85
RMSEC	7.47	6.38	5.71	7.27	5.98	5.82	6.18	6.61	5.57
RMSEV	6.06	5.13	4.84	5.78	4.58	4.21	5.95	5.53	4.22
RSD	5.0	2.8	2.8	4.0	5.6	4.6	3.1	4.2	3.9

RMSEC root mean square error of calibration, *RMSEV* root mean square error of validation, *RSD* relative standard deviation

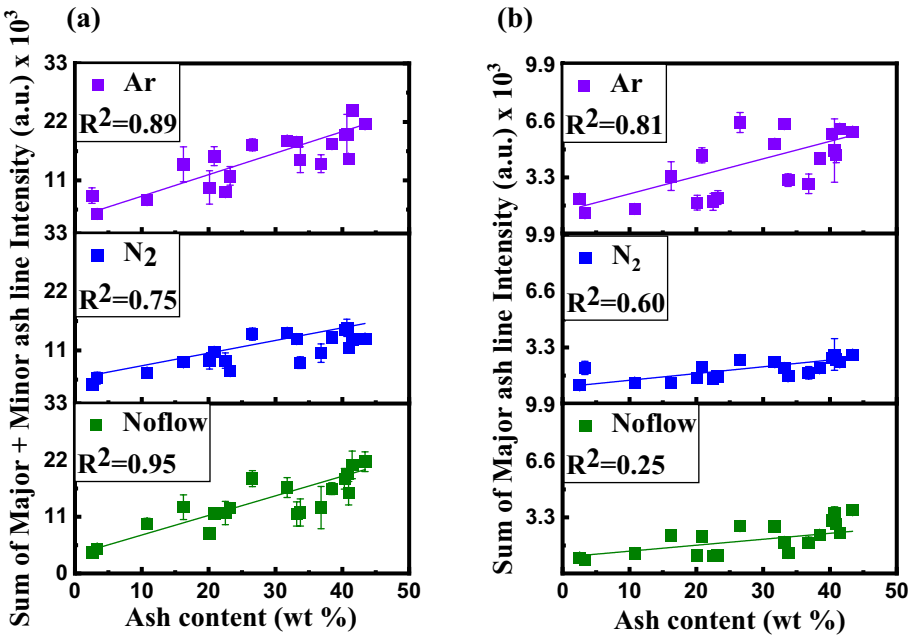

Fig. 7 Reference coal ash content versus **a** the sum of the intensities of major (Si, Fe, Al, and Ca) and the minor (Mg, Na, and K) ash forming elements and **b** the sum of the intensities of major ash forming elements

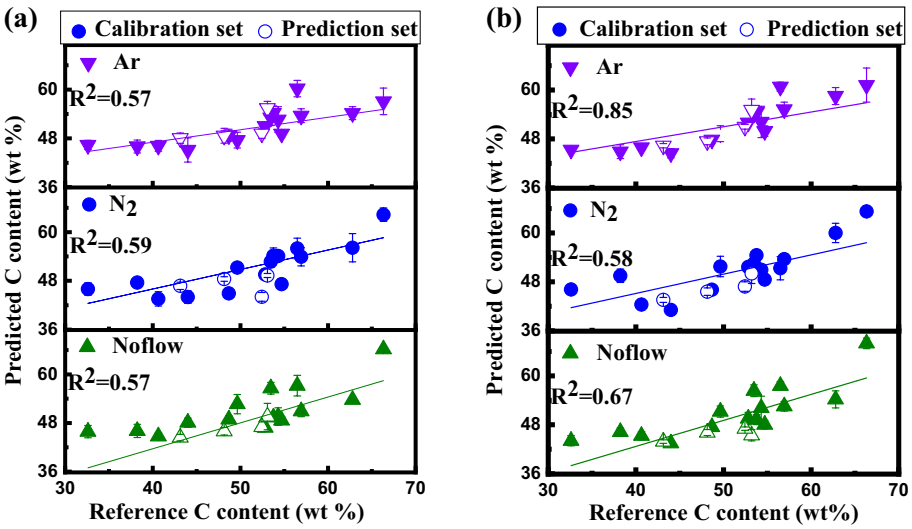

Fig. 8 Calibration plots using the ratio b/w the individual C emissions to the sum of emission intensities of **a** major and minor ash forming elements and **b** major ash forming elements under no flow, N_2, and Ar flow conditions using the PLSR method

RSD measurement values were improved when the ratio of the sum of emission intensities of all carbon emission lines and the sum of emission intensities of major ash elements was considered as compared to the sum of emission intensities of all ash elements. A few outliners in the calibration plot (Fig. 8) were attributed to the large variation of carbon wt% in the sample itself as confirmed by the C–H–N–S analysis. Also, the influence of the atmosphere on the C measurement was studied by comparing the results obtained by the last method at no flow, N_2, and Ar atmosphere. The R^2 of the fitting was measured as 0.67, 0.58, and 0.85; RMSEC was 5.71, 5.82, and 5.57; RMSEV was 4.84, 4.21, and 4.22; and RSD was 2.8, 4.6, and 3.9 at no flow, N_2, and Ar atmosphere, respectively. Hence, it can be concluded that the overall performance of the measurement technique was better in the case of the Ar environment than no flow and N_2 environment. The improvement in the LIBS-based analysis of coal was attributed to the Ar-induced plasma shielding effect, which alleviated the interaction of plasma with other atmospheric gas species resulting in the plasma emissions only from the target material and increases in the emission intensity.

In this analysis, the emission intensity of each inorganic element was considered entirely irrespective of its weight fraction in ash. However, the influence of variation in the number of constituents of each inorganic element in ash (based on its compositional wt% in ash) is also a critical parameter, and the measurement accuracy and sensitivity

are expected to improve by employing multivariate analysis incorporating weight fraction coefficient of each constituent.

4 Conclusion

In this work, the laser-induced breakdown spectroscopy (LIBS) technique is proposed and demonstrated for coal characterization in different gas environments with the controlled flow. The influence of different ambiances, namely atmospheric air, He, N_2, and Ar flow, on the measurement of carbon content during the LIBS analysis in free space is studied. Ar gas flow improved the atomic (C I, Si, Fe, Mg, Al, Ca, Na, and K) and molecular (CN and C_2) emissions, and N_2 gas flow enhanced the molecular carbon emissions (CN and C_2). The flow rate of any gas other than Ar gas does not influence the atomic and molecular C emissions (C I, CN, and C_2). Due to Ar-induced plasma shielding effect, the C emissions were reduced by increasing the Ar gas flow rate. Because of the larger atomic weight and density, the Ar environment results in plasma confinement and re-excitation of the plasma species. Hence, the optical signal strength, plasma temperature, and electron density are higher than that of in N_2, air, and He environment. The coal ash content of various coal samples can be directly related to the LIBS signal strength of the inorganic elements present in coal. The carbon emission signals alone were not sufficient enough to find the correlation between the LIBS spectrum of a coal sample with its reference carbon content using the PLSR method. Therefore, the heterogeneous nature of the coal samples was taken into account for the C measurement by considering the inorganic elemental lines. The sum of spectral intensities of all inorganic elements showed better linear fit w.r.t to the ash content than the sum of spectral intensities of major inorganic elements present in coal. The ratio between the carbon emissions and (a) the major and minor, and (b) only the major ash elements emissions showed a linearly increasing relationship with an increase in the carbon content. In that, the PLSR method involving the C and major ash elements resulted in better calibration with R^2—0.67, 0.58, and 0.85; RMSEC—5.71, 5.82, and 5.57; RMSEV—4.84, 4.21, and 4.22; RSD—2.8, 4.6, and 3.9 at no flow, N_2, and Ar atmosphere, respectively. A few outliners in the calibration analysis were attributed to the large variation of carbon wt% in the sample itself as confirmed by the C–H–N–S analysis. The improvement in the uniformity of carbon concentration in a coal sample under measurement will further enhance the LIBS performance in the Ar environment.

Acknowledgments The project was supported by the Grant-in-Aid from the UAY project (ASE1617134MUAYTMMU) with Bharat Heavy Electricals Limited (BHEL), India.

References

1. T. Erickson, S. Allan, D. McCollor, J. Hurley, S. Srinivasachar, S. Kang, J. Baker, M. Morgan, S. Johnson, R. Borio, Fuel Process Technol. **44**, 155 (1995)
2. M. Khandelwal, T. Singh, Fuel **89**, 1101 (2010)
3. J. Parus, J. Kierzek, B. Małżewska-Bućko, X-Ray Spectrom. **29**, 192 (2000)
4. L. Dep, M. Belbot, G. Vourvopoulos, S. Sudar, J. Radioanal. Nucl. Chem. **234**, 107 (1998)
5. D. Rusak, B. Castle, B. Smith, J. Winefordner, Crit. Rev. Anal. Chem. **27**, 257 (1997)
6. C.E. Romero, R.D. Saro, J. Craparo, A. Weisberg, R. Moreno, Z. Yao, Energy Fuel **24**, 510 (2009)
7. W. Li, J. Lu, M. Dong, S. Lu, J. Yu, S. Li, J. Huang, J. Liu, Energy Fuel **32**, 24 (2017)
8. W. Yin, B. Zhang, S. Jia, J. Test Measurement Technol. **4**, 356 (2011)
9. D. Body, B.L. Chadwick, Rev. Sci. Instrum. **72**, 1625 (2001)
10. S. Balakrishnan, V.M. Reddy, A. Mehta, N. Vasa, R. Nagarajan, Appl. Phys. A **122**, 399 (2016)
11. Q. Ma, P.J. Dagdigian, Anal. Bioanal. Chem. **400**, 3193 (2011)
12. M. Dong, X. Mao, J.J. Gonzalez, J. Lu, R.E. Russo, J. Anal. At. Spectrom. **27**, 2066 (2012)
13. X. Li, Z. Wang, Y. Fu, Z. Li, J. Liu, W. Ni, Appl. Spectrosc. **68**, 955 (2014)
14. S. Yao, J. Lu, M. Dong, K. Chen, J. Li, J. Li, Appl. Spectrosc. **65**, 1197 (2011)
15. N. Farid, S. Bashir, K. Mahmood, Phys. Scr. **85**, 015702 (2011)
16. L. Fornarini, V. Spizzichino, F. Colao, R. Fantoni, V. Lazic, Anal. Bioanal. Chem. **385**, 272 (2006)
17. P. Rohwetter, J. Yu, G. Méjean, K. Stelmaszczyk, E. Salmon, J. Kasparian, J.-P. Wolf, L. Wöste, J. Anal. At. Spectrom. **19**, 437 (2004)
18. Z. Wang, T.-B. Yuan, S.-L. Lui, Z.-Y. Hou, X.-W. Li, Z. Li, W.-D. Ni, Front. Phys. **7**, 708 (2012)
19. NIST LIBS database**,** https://physics.nist.gov/PhysRefData/ASD/LIBS/libs. Accessed 1 Oct 2019
20. S. Harilal, C. Bindhu, R.C. Issac, V. Nampoori, C. Vallabhan, J. Appl. Phys. **82**, 2140 (1997)
21. J.K. Antony, G.S. Jatana, N.J. Vasa, V.S. Raja, A. Laxmiprasad, Appl. Phys. A **101**, 161 (2010)
22. A. Shaltout, N. Mostafa, M. Abdel-Aal, H. Shaban, Eur. Phys. J. Appl. Phys. **50**, 1 (2010)
23. H.R. Griem, *Principles of Plasma Spectroscopy*, vol. vol 2 (Cambridge University Press, Cambridge, 2005)
24. M. Pishdast, A.E. Majd, M.K. Tehrani, Laser Part Beams **34**, 493 (2016)
25. S. Harilal, C. Bindhu, V. Nampoori, C. Vallabhan, Appl. Phys. Lett. **72**, 167 (1998)
26. F. Rezaei, S.H. Tavassoli, Spectrochim. Acta B **78**, 29 (2012)
27. S. Chakravarty, A. Mohanty, A. Banerjee, R. Tripathy, G. Mandal, M.R. Basariya, M. Sharma, Fuel **150**, 96 (2015)
28. W.J. Song, L.H. Tang, X.D. Zhu, Y.Q. Wu, Z.B. Zhu, S. Koyama, Energy Fuel **24**, 182 (2009)
29. M. Gaft, E. Dvir, H. Modiano, U. Schone, Spectrochim. Acta B **63**, 1177 (2008)